ISIJ International, Vol. 65 (2025), No. 13, pp. 2269–2274
https://doi.org/10.2355/isijinternational.ISIJINT-2025-334

Short Article

Thermodynamic Investigation of $MnAl_2O_4$ Spinel Precipitation Behavior in Manganese Containing-Slag Systems

Chonglin SHI,[1)]* Yuxing LIU,[1)] Kentaro URATA,[2)] Shintaro YASUI,[2)] Taichi ABE[3)] and Yoshinao KOBAYASHI[2)]

1) School of Materials and Chemical Technology, Institute of Science Tokyo, 2-12-1 Ookayama, Meguro-ku, Tokyo, 152-8550 Japan.
2) Laboratory for Zero-Carbon Energy, Institute of Integrated Research, Institute of Science Tokyo, 2-12-1 Ookayama, Meguro-ku, Tokyo, 152-8550 Japan.
3) Research Center for Structural Materials, National Institute for Materials Science, 1-2-1 Sengen, Tsukuba City, Ibaraki, 305-0047 Japan.

(*Received September 28, 2025; Accepted October 16, 2025; Advance online published October 29, 2025; Published December 15, 2025*)

In this study, the chemical equilibrium experiments were systematically conducted at 1 673 K under an oxygen partial pressure of 10^{-13} atm to investigate the precipitation of $MnAl_2O_4$ spinel in the $CaO–SiO_2–MgO–FeO–MnO–Al_2O_3$ slags. The results showed that with increasing Al_2O_3 content, Mn gradually transferred from the silicate liquid phase into the spinel phase. At 33.64 mol% Al_2O_3, the precipitation ratio of $MnAl_2O_4$ was approximately 80.32%, at which point the slag reached its solubility limit with respect to Al_2O_3. Therefore, 80.32% represented the maximum precipitation ratio attainable through Al_2O_3 control under the present experimental conditions. At this composition, comparison between water-quenching and slow cooling at 4 K/min revealed negligible differences in the crystal structure and composition of the spinel phase, indicating that $MnAl_2O_4$ precipitation predominately occurred during the high-temperature equilibration stage and remained stable upon cooling. In addition, with increasing Al_2O_3 content, the activity of MnO decreased, indicating its progressive consumption from the silicate melt and incorporation into the spinel phase.

KEY WORDS: thermodynamic analysis; $MnAl_2O_4$ spinel; $CaO–SiO_2–MgO–FeO–MnO–Al_2O_3$ slag; precipitation behavior; activity measurement.

1. Introduction

Manganese (Mn) steel is widely used in automotive, railway, and structural applications due to its excellent mechanical properties.[1,2)] With the increasing demand for high-performance steel, the production and application of Mn steel have continued to grow. According to the USGS Mineral Commodity Summaries 2024, global Mn mine production in 2023 was approximately 20 million tons, of which about 90% was consumed by the steelmaking industry.[3)] However, because of the strong affinity of Mn with oxygen, a substantial portion of Mn is inevitably lost to the slag during steelmaking. Material flow studies in Japan have shown that the amount of Mn used as an alloying element is nearly equivalent to the amount ultimately contained in the steelmaking slag.[4–6)] Statistics indicate that basic oxygen furnace (BOF) slag typically contains 2–6 mass% Mn, while electric arc furnace (EAF) slag may contain 5–10 mass% Mn.[7)] In Japan, 98.4% of steelmaking slag is reused, mainly as road base and civil engineering materials.[8)] Nevertheless, the reutilized slags still contain considerable amounts of Mn. Previous studies have shown that the phase assemblage in which major elements ultimately occur largely determines the reusability of slag,[9)] as it governs its long-term stability and mechanical properties. Therefore, it is necessary to systematically investigate the Mn-bearing phases in steel slags and their crystallization behavior.

Among the possible Mn-bearing phases, $MnAl_2O_4$ spinel not only forms readily in the slag but is also regarded as the most stable Mn-containing phase. Thus, clarifying the thermodynamic precipitation conditions of $MnAl_2O_4$ is particularly important, as it enables compositional control over its formation and enhances both the functionality and resource efficiency of slag reuse.

Nevertheless, studies on $MnAl_2O_4$ in the steelmaking process have so far mainly focused on $MnAl_2O_4$ inclusion

* Corresponding author: E-mail: shi.c.aa@m.titech.ac.jp

in steel,[10–14] while systematic studies on $MnAl_2O_4$ in steel slags remain very limited. By contrast, Cr and V-bearing spinels in slags have been extensively investigated, providing valuable insights. For Cr, the FeO content[15,16] and basicity[17] of the slag were found to strongly promote its incorporation into spinel, while Al_2O_3 additions could stabilize Cr in spinel.[18] In addition, cooling treatment has also been reported to further enhance Cr spinel formation.[19,20] For V, longer holding times and lower temperatures were shown to enhance the formation of V spinel in slags,[21] while higher FeO/SiO_2 ratios and MgO contents were found to promote MgV_2O_4 crystallization.[22] Despite these studies on spinel formation in slags, no systematic investigation has yet addressed $MnAl_2O_4$ in steel slags. In light of these gaps, clarifying the thermodynamic precipitation conditions of $MnAl_2O_4$ in steel slags could enable composition-based control over its generation, thereby enhancing the functionality and resource efficiency of slag reuse.

Therefore, this study focuses on the $CaO–SiO_2–MgO–FeO–MnO–Al_2O_3$ slags and aims to clarify the effects of varying Al_2O_3 content on the precipitation behavior of $MnAl_2O_4$ spinel through equilibrium experiments. On the basis of this, the influence of cooling conditions on the effect of Al_2O_3 addition was also investigated to comprehensively understand the precipitation behavior of $MnAl_2O_4$. In addition, the activities of MnO were also measured as part of the effort to better understand spinel precipitation behavior.

2. Experimental

2.1. Experimental Apparatus

The experimental apparatus is schematically shown in **Fig. 1**. An electric resistance furnace was equipped with $MoSi_2$ heating elements and an alumina tube reaction chamber. The isothermal zone was determined by the Pt/Pt-13Rh thermocouple with an accuracy of ± 1 K.

The chemical equilibrium process was conducted with an iron crucible which was placed on the refractory bricks in the alumina tube. The gas flow, consisting of argon (Ar) as the carrier gas and $CO–CO_2$ as reactive gases, together with the oxygen partial pressure, was regulated by the gas control system. Moreover, the Ar gas was further deoxidized using titanium in a deoxidizing furnace. The mixed gases were introduced from the top of the alumina tube and vented from the bottom.

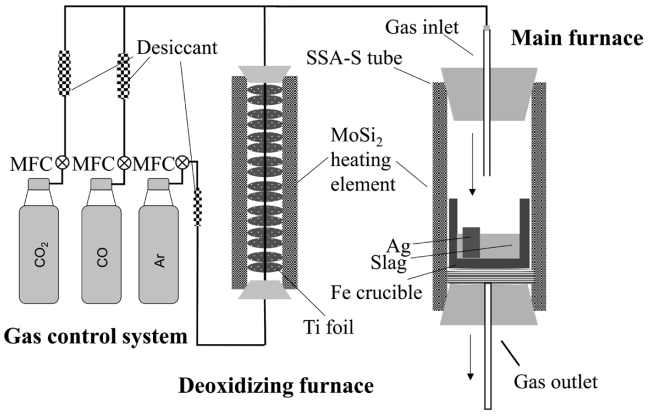

Fig. 1. Schematic diagram of the experimental apparatus.

2.2. Slag Preparation

The slag compositions in this study were designed based on a typical electric arc furnace (EAF) slag provided by a domestic Japanese steelmaking plant, with the initial chemical compositions summarized in **Table 1**, where Slag 2 represents the original slag. The Al_2O_3 content was varied while correspondingly adjusting the amounts of CaO and SiO_2 to maintain a constant basicity (CaO/SiO_2 molar ratio = 0.82).

To prepare CaO, $CaCO_3$ powder was calcined in an alumina crucible at 1 473 K (1 200°C) for 12 hours under an Ar atmosphere with a flow rate of 150 mL/min. Similarly, FeO was prepared by heating $FeC_2O_4·2H_2O$ at 1 273 K (1 000°C) for 6 hours under an Ar atmosphere with a flow rate of 300 mL/min.[23,24] The phase purity of both CaO and FeO was confirmed by XRD (Bruker D2 Phaser, 2nd generation).

The other raw materials, including MgO, MnO, SiO_2, and Al_2O_3, were mixed with the prepared CaO and FeO powders in predetermined ratios and ground uniformly using a planetary mono mill (Fritsch P-6S classic line, agate grinding ball). This homogenized powder mixture was used as the material for the thermodynamic equilibrium experiments.

2.3. Experimental Procedure

Thermodynamic equilibrium experiments were carried out to determine the activity of MnO in slags by equilibrating the slag with an Ag–Mn alloy. According to preliminary experiments, 28 hours of the holding time was long enough to reach equilibrium state. Each experiment was conducted at 1 673 K (1 400°C), using 8 g of pre-melted slag and 4 g of electrolytic silver (Ag, 99.99% purity), placed in an iron crucible. After equilibration, the samples were retrieved from the furnace and water-quenched immediately to obtain the Ag–Mn alloy and slag for analysis.

The oxygen partial pressure was precisely controlled at 10^{-13} atm by introducing a mixture of CO and CO_2 into the furnace chamber (at 1 673 K, $P_{CO}/P_{CO_2} \approx 151{:}1$).[25] This control method is based on the redox equilibrium between CO and CO_2,[26] represented by the following equations.

$$2CO(g) + O_2(g) = 2CO_2(g) \quad \text{..... (1)}$$

$$\Delta G^{\circ}_{(1)} = -561\,911 + 170.46T\,(\mathrm{J/mol}) \quad \text{..... (2)}$$

$$P_{O_2} = \exp\left(\frac{\Delta G^{\circ}_{(1)}}{RT}\right)\cdot\left(\frac{P_{CO_2}}{P_{CO}}\right)^2 \quad \text{..... (3)}$$

In Eq. (2), $\Delta G^{\circ}_{(1)}$ is the standard Gibbs energy change of reaction (1) at absolute temperature T. In Eq. (3), P_{O_2}, P_{CO} and P_{CO_2} are the partial pressures of O_2, CO and CO_2 respectively, and R is the gas constant (8.314 J/mol·K).

Table 1. Initial slag compositions (mol%). (All values in the following tables are given with four significant figures.)

No.	CaO	SiO_2	Al_2O_3	MgO	FeO	MnO
1	18.97	23.06	13.64	7.420	28.24	8.670
2	14.46	17.58	23.64	7.420	28.24	8.670
3	12.21	14.84	28.64	7.420	28.24	8.670
4	9.940	12.09	33.64	7.420	28.24	8.670

Table 2. Partial pressure ratios of CO_2 to CO required to maintain 10^{-13} atm oxygen partial pressure at different temperature intervals.

Interval (K)	P_{CO}/P_{CO_2}
1 673–1 633	121.0
1 633–1 593	77.74
1 593–1 553	49.51
1 553–1 513	31.34
1 513–1 473	19.62
1 473–1 433	11.90
1 433–1 393	6.940
1 393–1 353	3.863
1 353–1 313	2.062
1 313–1 273	0.4219

Additionally, to further clarify the precipitation behavior of $MnAl_2O_4$, additional experiments were conducted under controlled cooling conditions. Slag 4 was selected and subjected to slow cooling at a rate of 4 K/min after isothermal equilibration at 1 673 K for 28 hours. To maintain the oxygen partial pressure at 10^{-13} atm throughout the cooling process, the partial pressure ratio of CO_2 to CO was adjusted every 40 K (down to 1 273 K, since the slag had already solidified and further gas adjustment was unnecessary). This adjustment was determined by numerically integrating Eq. (4) to maintain the average oxygen partial pressure at 10^{-13} atm over the specified temperature range, and the corresponding partial pressure ratios of CO_2 to CO are summarized in **Table 2**.

$$\bar{p}_{O_2} = \frac{1}{T_{end} - T_{start}} \int_{T_{start}}^{T_{end}} \exp\left(\frac{\Delta G^{\circ}_{(1)}}{RT}\right) \cdot \left(P_{CO_2} / P_{CO}\right)^2 dT \quad \cdots (4)$$

2.4. Analysis

The morphology of the slag after the equilibrium experiment was examined by scanning electron microscopy equipped with energy-dispersive X-ray spectroscopy (SEM-EDS, JEOL JCM-7000). The chemical compositions of the individual phases in the slag were determined by SEM-EDS, and the overall phase identification was conducted by X-ray diffraction (XRD). The Mn concentration in the Ag–Mn alloy was measured by inductively coupled plasma optical emission spectroscopy (ICP-OES, HITACHI PS7800) after dissolution in nitric acid.

3. Results and Discussion

3.1. Thermodynamic Equilibrium Calculation of the $MnAl_2O_4$ Precipitation in the Slag

The precipitation reaction of $MnAl_2O_4$ spinel in slag and the corresponding Gibbs free energy change can be described as the following equations.

$$MnO + Al_2O_3 = MnAl_2O_4 \quad \cdots\cdots (5)$$

$$\Delta G_{(5)} = \Delta G^{\circ}_{(5)} + RT \ln \frac{a_{MnAl_2O_4}}{a_{MnO} \cdot a_{Al_2O_3}} \quad \cdots\cdots (6)$$

Table 3. Calculated activities of Al_2O_3 in slags.

No.	Al_2O_3 content (mol%)	$a_{Al_2O_3}$
1	13.64	0.3691
2	23.64	0.7203
3	28.64	0.8020
4	33.64	0.9374
5	36.56	1.000

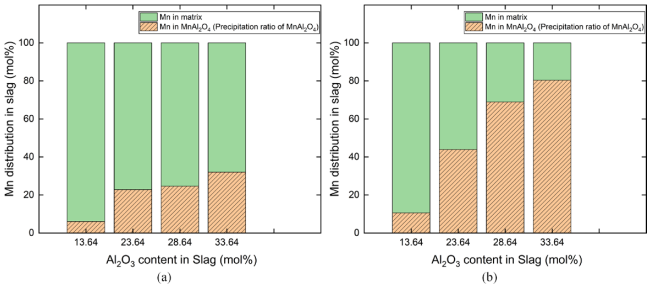

Fig. 2. Effect of Al_2O_3 content on Mn distribution in slags: (a) calculated results; (b) experimental results. (Online version in color.)

Since the activity of the precipitated spinel phase can be approximated as unity, the equilibrium driving force is mainly governed by the activities of MnO and Al_2O_3 in the slag. As what is shown in Eq. (6), increasing Al_2O_3 activity lowers $\Delta G_{(5)}$, shifting the equilibrium toward $MnAl_2O_4$ formation. This provides the thermodynamic basis for investigating the effect of Al_2O_3 content on spinel precipitation.

To evaluate this effect, equilibrium calculations were performed using FactSage 8.3 (FToxid 8.3 and FactPS 8.3 databases) under the same conditions as the experiments (1 673 K and an oxygen partial pressure of 10^{-13} atm). In the calculations, the molar fractions of MgO, FeO, and MnO were kept constant (7.420, 28.24, 8.670 mol% respectively), while the basicity was fixed at 0.82 to match the designed slags in Table 1. The calculated activities of Al_2O_3 are summarized in **Table 3**. With increasing bulk Al_2O_3, its activity increased progressively and reached unity at 36.56 mol%, indicating that the solubility limit had been reached.

The calculated Mn precipitation ratios are presented in **Fig. 2**(a). The precipitation ratio of $MnAl_2O_4$ was defined as the fraction of Mn incorporated into the spinel phase, relative to the total Mn content in the bulk slag. The addition of Al_2O_3 increased its activity in the slag. As a result, the fraction of Mn incorporated into the spinel phase was significantly enhanced. Accordingly, Al_2O_3 content was selected as the key compositional variable for the subsequent experiments.

3.2. Effect of Al_2O_3 Content on $MnAl_2O_4$ Precipitation

The SEM micrographs of Slag 1 to Slag 4 are shown in **Fig. 3**. Based on EDS compositional analysis, it was preliminarily identified that Slag 1–Slag 3 (Al_2O_3 = 13.64 to 28.64 mol%) consisted of three phases: a silicate/glassy matrix, metallic iron (Fe), and spinel. In Slag 4 (Al_2O_3 = 33.64 mol%), an Al_2O_3 phase was also observed. The XRD patterns shown in **Fig. 4** confirmed the above phase identification. For Slag 1 to Slag 3, the main crystalline phases

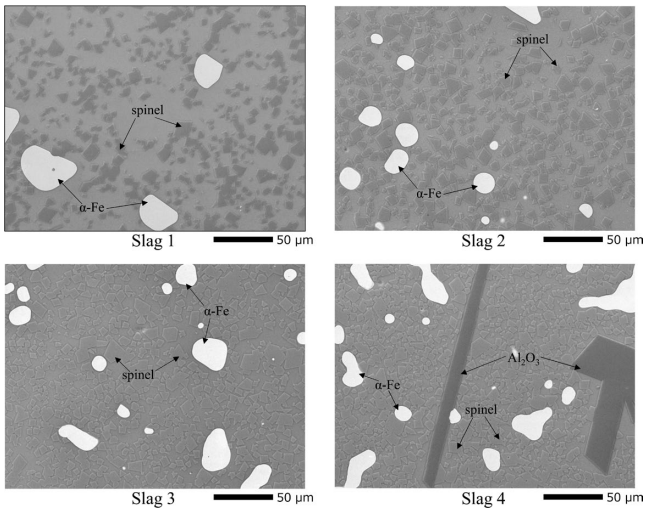

Fig. 3. SEM micrograghs for representive slag samples.

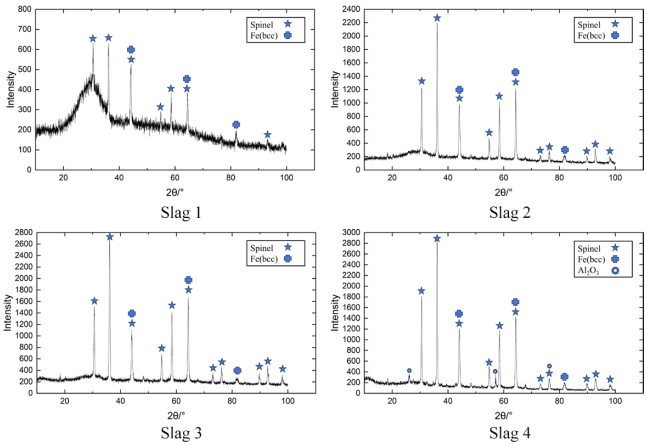

Fig. 4. XRD patterns of slags. (Online version in color.)

were spinel and metallic Fe, whereas Slag 4 exhibited not only spinel and metallic Fe but also minor diffraction peaks of Al_2O_3, suggesting that the content of Al_2O_3 exceeded the solubility limit of Al_2O_3 under the present condition. Moreover, from Slag 1 to Slag 4, with the gradual increase of Al_2O_3 content, the broad amorphous hump between 25° and 37° (2θ), corresponding to the diffraction of the glassy matrix phase, gradually diminished and eventually disappeared, while the spinel peaks intensified, suggesting a relative decrease of the glassy matrix and enrichment of the spinel phase. Furthermore, the chemical compositions of the spinel and matrix phase, determined by EDS, are summarized in **Table 4**. For spinel phase, the cation ratio (Mg+Fe+Mn):Al was approximately 1:2, consistent with the stoichiometry of spinel-type oxides (AB_2O_4), confirming that the spinel phase is a solid solution of $MnAl_2O_4$, $FeAl_2O_4$, and $MgAl_2O_4$. Moreover, silicon (Si) was detected only in the matrix phase, whereas Mn was found exclusively in the spinel and matrix phases (despite the presence of Mn in the Ag–Mn alloy, with a concentration of no more than 0.153 mol%, it was considered negligible and not included in the analysis). Accordingly, the relative amounts of matrix and spinel, as well as the precipitation ratio of $MnAl_2O_4$, were calculated based on elemental balances using the following equations.

Table 4. Chemical composition of spinel and matrix phases determined by EDS (mol%).

No.	Phase	O	Ca	Si	Al	Mg	Fe	Mn
1	Spinel	49.25	–	–	34.23	10.28	2.131	4.110
	Matrix	51.93	12.00	14.84	12.02	2.544	1.686	4.989
2	Spinel	48.42	–	–	34.30	6.473	5.420	5.390
	Matrix	51.58	12.06	14.44	14.29	0.8600	2.846	3.996
3	Spinel	50.55	–	–	33.45	5.360	5.935	4.700
	Matrix	53.66	11.83	14.36	14.48	0.3770	2.681	2.610
4	Spinel	48.89	–	–	34.60	4.670	6.410	5.430
	Matrix	53.08	11.68	13.96	18.06	0.07800	1.170	1.970

$$N_{\text{matrix}} = \frac{N_{\text{Si}}^{\text{bulk}}}{X_{\text{Si}}^{\text{matrix}}} \quad \text{..... (7)}$$

$$N_{\text{spinel}} = \frac{N_{\text{Mn}}^{\text{bulk}} - N_{\text{matrix}} \cdot X_{\text{Mn}}^{\text{matrix}}}{X_{\text{Mn}}^{\text{spinel}}} \quad \text{..... (8)}$$

$$R_{\text{MnAl}_2\text{O}_4} = \frac{N_{\text{spinel}} \cdot X_{\text{Mn}}^{\text{spinel}}}{N_{\text{Mn}}^{\text{bulk}}} \quad \text{..... (9)}$$

$N_{\text{Mn}}^{\text{bulk}}$ and $N_{\text{Si}}^{\text{bulk}}$ denote the total moles of Mn and Si in the bulk slag, while $X_{\text{Mn}}^{\text{matrix}}$, $X_{\text{Si}}^{\text{matrix}}$ and $X_{\text{Mn}}^{\text{spinel}}$ represent the average molar fractions of elements in the respective phases determined by EDS. N_{matrix} and N_{spinel} are the relative amounts of the matrix and spinel phase, and $R_{\text{MnAl}_2\text{O}_4}$ is the precipitation ratio of $MnAl_2O_4$, defined as the fraction of Mn incorporated into the spinel phase relative to the total Mn content in the bulk slag. In this study, since the dissolution of spinel-rich slags was incomplete in ICP-OES analysis, the total moles of Mn and Si in the bulk slag used in the balance calculations were taken directly from the initial charge.

The ratio of spinel to the glassy matrix phase ($N_{\text{spinel}}/N_{\text{matrix}}$) shows an increasing trend with Al_2O_3 content, which is consistent with the XRD results. Mn distribution in slags at different Al_2O_3 contents is shown in Fig. 2(b). The results show that the precipitation ratio of $MnAl_2O_4$ increased with increasing Al_2O_3 content and reached a maximum of 80.32% at 33.64 mol% Al_2O_3, at which point the slag became saturated with Al_2O_3. Owing to this saturation effect, further additions of Al_2O_3 did not lead to any increase in the precipitation ratio. Therefore, under the present experimental conditions, 33.64 mol% Al_2O_3 can be regarded as the optimum composition for achieving the maximum precipitation ratio of $MnAl_2O_4$ spinel (80.32%). This behavior is consistent with the evaluation in Section 3.1: as Al_2O_3 content increases, its activity rises, shifting the equilibrium of reaction (5) toward spinel formation and thereby increasing the precipitation ratio of $MnAl_2O_4$ spinel. Although the activity of Al_2O_3 is difficult to measure directly due to its strong stability, the experimental observation of Al_2O_3 saturation (Al_2O_3 activity→1) substantiates this interpretation. It should be noted that quantitative discrepancies remain between experiment and calculation. At the same bulk Al_2O_3 contents, the experimental precipitation ratios were generally higher than the calculated values, and the onset of Al_2O_3 saturation occurred earlier than predicted.

These deviations are mainly due to the lack of prior studies, which has limited the completeness of the FactSage thermodynamic database for the present system. Nevertheless, the calculations reproduced the overall experimental trend, indicating their reliability. The present results can provide a thermodynamic supplement and extend the applicability of thermodynamic predictions to Mn-bearing spinel precipitation in this system.

3.3. Effect of Cooling Rate on $MnAl_2O_4$ Precipitation

In industrial practice, steel slag is commonly subjected to various cooling methods, including slow cooling, water cooling, and air cooling.[27,28] As noted in the introduction, previous studies have demonstrated that cooling conditions are known to affect spinel precipitation, such as crystal growth, crystallization sequence, and the precipitation ratio of specific element-bearing spinels.[12,15–19] To examine whether such effects occur under the present conditions, the slag with 33.64 mol% Al_2O_3 was first equilibrated at 1 673 K for 28 h under an oxygen partial pressure of 10^{-13} atm. The sample was then subjected to slow cooling at 4 K/min, and the results were compared with those obtained from the sample quenched immediately after equilibration. SEM, XRD, and EDS analyses revealed that the spinel phase obtained under both conditions exhibited nearly identical compositions (**Table 5**). Furthermore, the principal diffraction peaks of spinel in the XRD patterns showed almost no shift in 2θ positions (**Fig. 5**), confirming that the crystal structure was essentially unchanged with the cooling method.

This phenomenon can be explained from both thermodynamic and kinetic perspectives. For the reaction given in Eq. (5), the Gibbs free energy change of $MnAl_2O_4$ formation,[29] expressed in Eq. (10), decreases with decreasing temperature, indicating that the spinel phase remains thermodynamically stable during cooling. Meanwhile, since most Mn in the liquid phase had already been consumed during the high-temperature equilibration stage and diffusion rates decreased significantly upon cooling, further nucleation of spinel was kinetically unfavorable.

In summary, the cooling method (quenching vs. slow cooling) had no significant effect on the $MnAl_2O_4$ precipitated during the high-temperature equilibrium stage, which indicates that $MnAl_2O_4$ maintains its stability under different cooling conditions once equilibrium precipitation has been achieved.

$$\Delta G^{\circ}_{(5)} = -45\,116 + 11.81T\,(\mathrm{J/mol}) \quad \text{..... (10)}$$

3.4. Effect of Al_2O_3 Content on the Activity of MnO in Slag

The activity of MnO is defined as its thermodynamically effective concentration in the slag melt. Unlike the simple concentration, activity reflects the actual chemical potential of MnO in the system and therefore determines its ability to participate in reactions. When the activity of MnO in the slag system decreases, it indicates that the free MnO in the melt is being progressively consumed, for example, through incorporation into the spinel phase. Therefore, measuring the activity of MnO under different Al_2O_3 contents can directly reveal the thermodynamic driving force for

Table 5. Comparison of spinel compositions after slow cooling and quenching determined by EDS (mol%).

Cooling method	O	Al	Mg	Fe	Mn
quenching	48.89	34.60	4.670	6.410	5.430
slow cooling	48.24	35.18	4.506	6.572	5.502

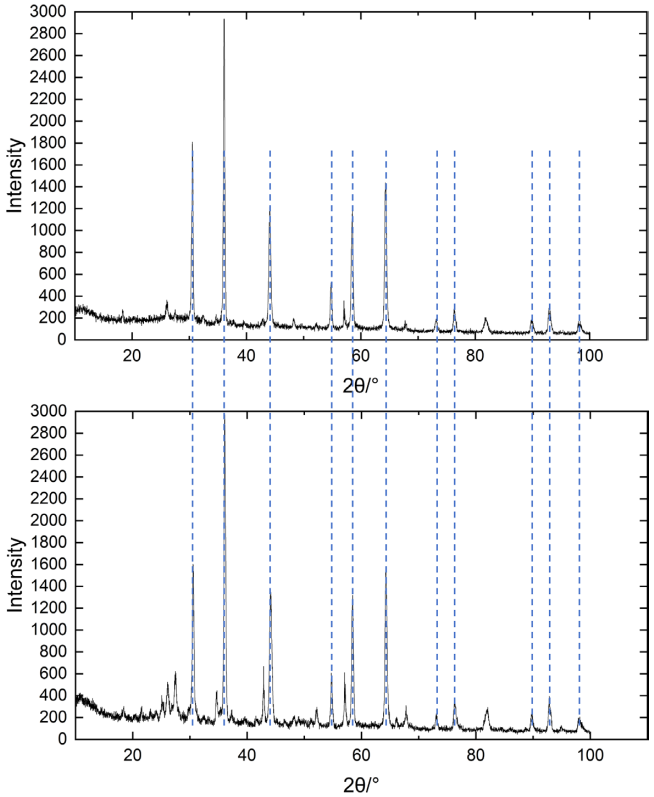

Fig. 5. Comparison of XRD patterns of spinel phases under water-quenching (a) and slow cooling (4 K/min) (b). (Online version in color.)

$MnAl_2O_4$ formation. In this study, the activities of MnO were determined by using the chemical equilibrium method with an Ag–Mn alloy as the reference metal at 1 673 K and 10^{-13} atm oxygen partial pressure in the $CaO–SiO_2–MgO–FeO–MnO–Al_2O_3$ slags with varying Al_2O_3 contents. These data not only provided valuable insights into the formation mechanism of $MnAl_2O_4$ but also served as important thermodynamic supplements for this complex system, contributing to improved accuracy in future thermodynamic calculations. The activity of MnO, which is expressed as a_{MnO} can be calculated from its oxidation reactions and the corresponding standard Gibbs energy changes,[21] which are shown as the following equations.

$$\mathrm{Mn(l)} + \frac{1}{2}\mathrm{O_2(g)} = \mathrm{MnO(s)} \quad \text{..... (11)}$$

$$\Delta G^{\circ}_{(11)} = -400\,995 + 84.27T\,(\mathrm{J/mol}) \quad \text{..... (12)}$$

$$a_{MnO} = \exp\left(\frac{-\Delta G^{\circ}_{(11)}}{RT}\right)\cdot\gamma_{Mn}\cdot X_{Mn}\cdot P_{O_2}^{\frac{1}{2}} \quad \text{..... (13)}$$

$$\log\gamma^{\circ}_{Mn\ in\ Ag(l)} = \frac{-2\,132}{T} + 1.088 \quad \text{..... (14)}$$

In Eq. (13), X_{Mn} is the mole fraction of Mn in the Ag–Mn

Table 6. Activities of MnO in slags.

No.	Al_2O_3 content (mol%)	X_{Mn}	a_{MnO}
1	13.64	0.001530	0.04137
2	23.64	0.001170	0.03164
3	28.64	0.001052	0.02845
4	33.64	0.0007829	0.02117

alloy, and γ_{Mn} denotes the activity coefficient of Mn in the Ag–Mn alloy. Under dilute conditions, γ_{Mn} can be regarded as equivalent to the Raoultian activity coefficient of Mn at infinite dilution in liquid Ag, as given by Eq. (14).[30] The activities of MnO calculated from the method described above along with the corresponding mole fractions of Mn in the Ag–Mn alloy were summarized in **Table 6**. With increasing Al_2O_3 content, the activity of MnO decreased, while, as observed in Section 3.2, the precipitation ratio of Mn spinel increased. This indicates that the free MnO dissolved in the silicate melt (which solidified into the glassy matrix upon cooling) was continuously consumed to form the spinel phase. The variation trend of MnO activity provides thermodynamic support for the formation of $MnAl_2O_4$.

4. Conclusions

In the present work, thermodynamic equilibrium experiments were conducted at 1 673 K under an oxygen partial pressure of 10^{-13} atm to investigate the precipitation behavior of $MnAl_2O_4$ spinel in the CaO–SiO_2–MgO–FeO–MnO–Al_2O_3 slags. The main conclusions are as follows:

(1) With increasing Al_2O_3 content from 13.64 mol% to 33.64 mol%, Mn gradually transferred from the silicate liquid phase into the spinel phase. At 33.64 mol% Al_2O_3, the precipitation ratio of $MnAl_2O_4$ was approximately 80.32%, at which point the slag reached its solubility limit with respect to Al_2O_3. Therefore, the maximum precipitation ratio of $MnAl_2O_4$ was achieved under this condition.

(2) At 33.64 mol% Al_2O_3, comparison between quenching and slow cooling at 4 K/min revealed negligible differences in the crystal structure and composition of the spinel phase, indicating that $MnAl_2O_4$ precipitation was mainly completed during the high-temperature equilibration stage and remained stable upon cooling.

(3) With increasing Al_2O_3 content, the activity of MnO decreased, indicating that MnO originally dissolved in the silicate melt (later solidified as the glassy matrix) was progressively consumed and incorporated into the spinel phase.

(4) From a practical perspective, controlling the Al_2O_3 content effectively facilitates the precipitation of Mn in the form of $MnAl_2O_4$ spinel. This provides a thermodynamic basis and support for regulating the chemical state of Mn in slag and improving the utilization of steelmaking slags.

Statement for Conflict of Interest

The authors declare that there are no conflicts of interest regarding this study.

Acknowledgment

The authors are grateful to the research group of "Analysis of the Existence State of Mn in Steelmaking Slags" at the Iron and Steel Institute of Japan (ISIJ) for their financial support.

REFERENCES

1) R. Zellagui, L. Hemmouche, H. Ait-Sadi and A. Chelli: *Arch. Metall. Mater.*, **67** (2022), 863. https://doi.org/10.24425/amm.2022.139676
2) S. J. Kim, J. Takekawa, H. Shibata, S. Y. Kitamura, K. Yamaguchi and Y. B. Kang: *ISIJ Int.*, **53** (2013), 1325. https://doi.org/10.2355/isijinternational.53.1325
3) United States Geological Survey: Manganese Statistics and Information, https://www.usgs.gov/centers/national-minerals-information-center/manganese-statistics-and-information, (accessed 2025-07-25).
4) K. Nakajima, K. Yokoyama and T. Nagasaka: *ISIJ Int.*, **48** (2008), 549. https://doi.org/10.2355/isijinternational.48.549
5) S. Kim, H. Shibata, N. Maruoka, S. Kitamura and K. Yamaguchi: *High Temp. Mater. Process.*, **30** (2011), 425. https://doi.org/10.1515/htmp.2011.064
6) S. Kim, J. Suzuki, X. Gao, S. Ueda and S. Kitamura: *J. Sustain. Metall.*, **2** (2016), 141. https://doi.org/10.1007/s40831-016-0042-z
7) Y. Huang, G. Xu, H. Cheng, J. Wang, Y. Wan and H. Chen: *Procedia Environ. Sci.*, **16** (2012), 791. https://doi.org/10.1016/j.proenv.2012.10.108
8) Nippon Slag Association: Iron and Steel Slag (2022), https://www.slg.jp/statistics/report.html, (accessed 2025-05-09).
9) L. Jiang, Y. Bao, Q. Yang, Y. Chen, G. Liu, F. Han, J. Wei, F. Engström and J. Deng: *Steel Res. Int.*, **88** (2017), 1700066. https://doi.org/10.1002/srin.201700066
10) Z. Y. Deng and M. Y. Zhu: *ISIJ Int.*, **53** (2013), 450. https://doi.org/10.2355/isijinternational.53.450
11) M. K. Paek, J. M. Jang, M. Jiang and J. J. Pak: *ISIJ Int.*, **53** (2013), 973. https://doi.org/10.2355/isijinternational.53.973
12) L. Z. Kong, Z. Y. Deng and M. Y. Zhu: *ISIJ Int.*, **57** (2017), 1537. https://doi.org/10.2355/isijinternational.ISIJINT-2017-118
13) Z. Y. Deng, Z. H. Liu, M. Y. Zhu and L. Q. Huo: *ISIJ Int.*, **61** (2021), 1. https://doi.org/10.2355/isijinternational.ISIJINT-2020-352
14) Y. Wang, Y. Yang, Z. Dong, J. Park, Z. Mi, X. Mao and W. Mu: *Metall. Mater. Trans. B*, **53** (2022), 2182. https://doi.org/10.1007/s11663-022-02517-2
15) J. Li, A. Xu, D. He, Q. Yang and N. Tian: *Int. J. Miner. Metall. Mater.*, **20** (2013), 253. https://doi.org/10.1007/s12613-013-0720-9
16) Q. Zeng, J. Li, Q. Mou, H. Zhu and Z. Xue: *JOM*, **71** (2019), 2331. https://doi.org/10.1007/s11837-019-03465-0
17) X. Wu, X. Dong, R. Wang, H. Lv, F. Cao and X. Shen: *J. Residuals Sci. Technol.*, **13** (2016), S57. https://doi.org/10.12783/issn.1544-8053/13/2/S10
18) Z. Wang and I. Sohn: *Ceram. Int.*, **47** (2021), 10918. https://doi.org/10.1016/j.ceramint.2020.12.211
19) L. Cao, C. Liu, Q. Zhao and M. Jiang: *J. Iron Steel Res. Int.*, **25** (2018), 1131. https://doi.org/10.1007/s42243-018-0058-7
20) Y. Yu, J. Li, M. Li and Z. Xue: *J. Min. Mater. Charact. Eng.*, **5** (2017), 132. https://doi.org/10.4236/jmmce.2017.53011
21) W. Huang and Y. Liu: *ISIJ Int.*, **60** (2020), 2183. https://doi.org/10.2355/isijinternational.ISIJINT-2020-039
22) J. Diao, H. Tao, Z. Lai, Y. Qiu, L. Chen, H. Li and B. Xie: *CrystEngComm*, **26** (2024), 2248. https://doi.org/10.1039/d4ce00189c
23) Y. Shen, J. Chong, Z. Huang, J. Tian, W. Zhang, X. Tang, W. Ding and X. Du: *Mater.* (*Basel*), **12** (2019), 2562. https://doi.org/10.3390/ma12162562
24) Y. Gao, C. Duan, Y. Yang, D. Ruan, C. Yang and C. Hong: *ISIJ Int.*, **55** (2015), 2273. https://doi.org/10.2355/isijinternational.ISIJINT-2014-826
25) X. Lu, T. Miki and T. Nagasaka: *Int. J. Miner. Metall. Mater.*, **24** (2017), 25. https://doi.org/10.1007/s12613-017-1375-8
26) E. T. Turkdogan: Physical Chemistry of High Temperature Technology, Academic Press, New York, (1980), 7.
27) K. Schollbach, M. J. Ahmed and S. R. van der Laan: *Int. J. Ceram. Eng. Sci.*, **3** (2021), 21. https://doi.org/10.1002/ces2.10078
28) Y. Li, K. Guo, J. Xiang, Y. Wang, W. Guo and S. Zhang: *ISIJ Int.*, **62** (2022), 2197. https://doi.org/10.2355/isijinternational.ISIJINT-2022-229
29) M. Timucin and A. Muan: *J. Am. Ceram. Soc.*, **75** (1992), 1399. https://doi.org/10.1111/j.1151-2916.1992.tb04200.x
30) S. C. Shim, F. Tsukihashi and N. Sano: *Metall. Trans. B*, **24** (1993), 333. https://doi.org/10.1007/BF02659136